

## Noise-induced sidebranching in the three-dimensional nonaxisymmetric dendritic growth

Efim Brener\* and Dmitri Temkin†

*Institut für Festkörperforschung, Forschungszentrum Jülich, D-52425 Jülich, Germany*

(Received 12 April 1994)

We consider the time-dependent behavior of sidebranching deformations taking into account the actual nonaxisymmetric shape of the needle crystal. The Green's function of the linearized problem is presented by a functional integral with the help of the Mullins-Sekerka local spectrum. For the short-wavelength perturbations the functional integral can be calculated by the steepest descent method, where the Green's function behavior is determined by the extremal trajectories governed by Hamilton equations. The local spectrum plays the role of the Hamilton's function. As in the axisymmetric approach [J.S. Langer, *Phys. Rev. A* **36**, 3350 (1987)], noise-induced wave packets generated in the tip region grow in amplitude, and spread and stretch as they move down the sides of the dendrite producing a train of sidebranches. The amplitude grows exponentially as a function of  $(|Z|^{2/5}/\sigma^{1/2})$ , where  $|Z|$  is the distance from the dendritic tip and  $\sigma$  is the stability parameter. The important result is that the amplitude of the sidebranches for the anisotropic needle crystal grows faster than for the axisymmetric paraboloid shape [in the latter case it grows exponentially but only as a function of  $(|Z|^{1/4}/\sigma^{1/2})$ ]. We argue that this effect can resolve the puzzle that experimentally observed sidebranches have much larger amplitudes than can be explained by thermal noise in the framework of the axisymmetric approach. The coarsening behavior of sidebranches in the nonlinear regime is briefly discussed.

PACS number(s): 44.30.+v, 68.45.-v, 81.30.Fb

### I. INTRODUCTION

During the past few years, our understanding of pattern formation in various nonlinear dissipative systems has made remarkable progress. Building on these foundations, it has now become possible to develop a description of a large class of patterns that are found in diffusional growth. Recently, much progress has been made on the question of what determines the structure of dendritic crystals [1]. It has become clear that the degeneracy of the macroscopic problem (family of Ivantsov parabolas [2]) is lifted by surface tension acting as a singular perturbation. Most surprisingly, this selection mechanism is beyond all orders of perturbation theory; therefore, it requires a rather sophisticated analysis to reveal its working. One outcome of this theory is the critical importance of crystalline anisotropy. But a physical anisotropy, say, with an underlying cubic symmetry, will give rise to a nonaxisymmetric crystal shape in three-dimensional (3D) dendritic growth. This makes the problem more difficult to solve compared with the two-dimensional (2D) case.

Recently, an analytical theory of the needle crystal in the 3D dendritic growth has been developed by Ben Amar and Brener [3] and by Brener [4]. The term "needle crystal" came from the idea that the crystal shape should be

close to the Ivantsov paraboloid. It turned out to be true only in the tip region of the dendrite [4]. The cross section of the interface in the tail region is represented by four well-developed (for cubic anisotropy) arms. The length and width of the arms increase as  $|z|^{3/5}$  and  $|z|^{2/5}$ , respectively, where  $|z|$  is the distance from the dendritic tip (in contrast with paraboloid, where the radius of the cross section increases as  $|z|^{1/2}$ ). This intermediate asymptotics should hold as long as the diffusion length for the side growth of the arms is larger than the size of the arms, before a subsequent crossover to the classical constant velocity regime of the 2D dendritic growth of the arms. In this last regime the length of the arms increases as  $|z|$ . This anisotropic crystal shape agrees reasonably well with the experimental observations [5–8].

Clearly, this steady-state solution [4] does not account for the noise-induced sidebranching behavior. The description of this behavior necessitates the solution of a time-dependent problem for the noise-induced perturbation about the needle-crystal shape. Langer and co-workers [9–11] suggested that dendritic sidebranches might be generated by selective amplification of a very small, noisy perturbation near the tip of a growing needle crystal. It appeared that realistic sidebranching behavior might be produced by purely thermal fluctuations in the solidifying material. The original argument [9] was based on the local boundary model of solidification, but later [11], all results were presented in terms of the more realistic, fully nonlocal, 3D model of solidification. In contrast to the boundary-layer model, the nonlocal model is based on a completely realistic description of the thermal field; thus, thermal fluctuations have been added to the

\*Permanent address: Institute for Solid State Physics, Academy of Sciences, 142432 Chernogolovka, Russia.

†Permanent address: Institute of Physical Metallurgy, 2 Baumanskaya Str., 9/23, 107005 Moscow, Russia.

problem in a very elegant and rigorous way.

The basic result presents the way in which a localized disturbance grows and propagates down the side of the dendrite. This disturbance is described in [11] as a small (linear) perturbation moving on a cylindrically symmetric steady-state needle crystal (Ivantsov paraboloid). The wave packet continues to grow at arbitrarily large distances down the dendrite. In the linear approximation, growth is exponential, but the exponent is proportional to  $|z|^{1/4}$ . The small power law is the result of the fact that only components of lower and lower frequency in the initial pulse continue to grow unstably as  $|z|$  becomes large. These results are in approximate, qualitative agreement with available experimental observations [5,6], but experimentally observed sidebranches have much larger amplitudes than explicable by thermal noise in the framework of the axisymmetric approach [11]. It means that either the thermal fluctuation strength turns out not to be quite adequate to produce visible sidebranching deformations, or agreement with experiment would require at least one more order of magnitude in the exponential amplification factor.

The main aim of this paper is to describe the sidebranching problem taking into account the actual non-axisymmetric shape of the needle crystal. Brener [4] has already mentioned that the amplification factor depends on the needle-crystal shape and for the actual non-axisymmetric shape this factor should be larger, because the length of the main arms grows as  $|z|^{3/5}$ , which is faster than  $|z|^{1/2}$  for Ivantsov paraboloid. We will show that this idea allows one to remove the above-mentioned discrepancy between the theory and experiment. We also want to focus on the analytic aspects of this theory because they turn out to be very interesting, especially for the nonaxisymmetric problem. We use the analytic approach which has been developed in Ref. [12] and which is slightly different from the approach of Refs. [10,11]. The starting point of this approach is the representation of the Green's function of the linear operator by a functional integral with a help of the local spectrum of the operator [13]. For the short-wavelength perturbations the functional integral can be calculated by the steepest descent method, where the Green's function behavior is determined by the extremal trajectories governed by Hamilton equations. The local spectrum plays the role of the Hamilton's function in this mechanical analogy. In this approach we can take advantage of the local spectrum of our problem; it is just the well-known Mullins-Sekerka spectrum. For the already investigated 2D and 3D axisymmetric cases, both approaches [10,11] and [12] give the same results.

## II. FORMULATION OF THE PROBLEM

Let us study the problem of a free dendrite growing in a one-component undercooled melt. The control parameter is the dimensionless undercooling  $\Delta = (T_M - T_\infty)c_p/L$ , where  $T_M$  is the melting temperature,  $L$  the latent heat, and  $c_p$  the specific heat. The temperature field satis-

fies the diffusion equation with the interface moving with normal velocity  $v_n$  and acting as a source of magnitude  $v_n L/c_p$ . Together with the Gibbs-Thomson condition at the interface, it leads to a rather complicated integral-differential evolution equation.

The steady-state version of this problem has been discussed in Refs. [3,4]. The dendritic tip with the radius of curvature  $\rho$  moves at a constant velocity  $v$ . The Peclet number  $P = \rho v/2D$  ( $D$  is the thermal diffusivity) is related to the undercooling  $\Delta$  by the 3D Ivantsov formula [2], which reads for small  $\Delta$

$$P(\Delta) = -\Delta/\ln \Delta. \quad (1)$$

The stability parameter  $\sigma$  is given by

$$\sigma \equiv d_0/(P\rho) = \sigma^*(\alpha), \quad (2)$$

where  $d_0 = \gamma T_M c_p/L^2$  is the capillary length proportional to the isotropic part of the surface energy  $\gamma$  and  $\alpha$  is the strength of the crystalline anisotropy. The function  $\sigma^*(\alpha)$  is given by the 3D selection theory [3] and  $\sigma^*(\alpha) \propto \alpha^{7/4}$  for small  $\alpha$ . Relation (2) together with the Ivantsov relation (1) determines both  $v$  and  $\rho$ . The interface shape in the tip region is close to the Ivantsov paraboloid and can be described by the equation [14]

$$z(r, \phi) = -\frac{r^2}{2} + \sum A_m r^m \cos(m\phi), \quad (3)$$

with the amplitudes  $A_m$  given by the 3D selection theory [3]. It is convenient from the beginning to measure all lengths in units of  $\rho$  and all times in units of  $\rho/v$ . In the tail region the interface shape deviates from the Ivantsov paraboloid: four well-developed arms (for cubic symmetry) are formed in the cross section. For small  $\Delta$ , not too far from the tip, this shape can be described as [4]

$$y(x, z) = (5|z|/3)^{2/5} \left( \frac{\sigma^*}{\sigma_2^*} \right)^{1/5} \left( \frac{x}{x_{tip}} \right)^{2/3} \times \int_{x/x_{tip}}^1 \frac{ds}{s^{2/3} \sqrt{1-s^4}}, \quad (4)$$

where the tip position of the arm  $x_{tip}$  is given by

$$x_{tip}(z) = (5|z|/3)^{3/5} (\sigma_2^*/\sigma^*)^{1/5}. \quad (5)$$

The function  $\sigma_2^*(\alpha)$  is given by the 2D selection theory and the ratio  $\sigma_2^*(\alpha)/\sigma^*(\alpha)$  is independent of  $\alpha$  in the limit of small  $\alpha$ . This means that the shape (4),(5) in the tail region is almost independent of the material and growth parameters, as well as the shape (3) in the tip region (if all the lengths are reduced by  $\rho$ ).

### A. Green's function of propagating perturbations

The description of the sidebranches necessitates the solution of a time-dependent problem for the perturba-

tion about the missile-shaped steady-state crystal  $z = \zeta_0(x, y)$ . As in Ref. [11], we assume this perturbation to be small and consider its evolution in the linear approximation. Therefore, the first step in this analysis is to linearize the evolution equation about the steady-state

solution. For the investigation of the behavior of a noise-induced wave packet as it moves along the dendrite it is important to know the Green's function of our linear problem. According to Ref. [13], the Green's function is given by a path integral,

$$G(X, Y, t, X', Y', t') = \int \exp \left[ \int_{t'}^t \Omega(x, y, k_x, k_y) d\tau - i \int_{X'}^X k_x dx - i \int_{Y'}^Y k_y dy \right] D\{x(\tau)\} D\{y(\tau)\} \times D\{k_x(\tau)\} D\{k_y(\tau)\}. \quad (6)$$

Here the functional integration is performed over all the trajectories  $x(\tau)$ ,  $y(\tau)$ ,  $k_x(\tau)$ , and  $k_y(\tau)$ , which start at the point  $x = X', y = Y'$  at  $\tau = t'$  and come to the point  $x = X, y = Y$  at  $\tau = t$ . The Green's function  $G$  describes the perturbation of the interface at an arbitrary point  $X, Y, Z = \zeta_0(X, Y)$  at time  $t$  as a response to the initially  $\delta$ -localized perturbation of the interface at the point  $X', Y', Z' = \zeta_0(X', Y')$  at time  $t'$ .

The expression for the Green's function is of the Feynman type, but with the action

$$S = \int_{t'}^t \Omega(x, y, k_x, k_y) d\tau - i \int_{X'}^X k_x dx - i \int_{Y'}^Y k_y dy \quad (7)$$

written in the Hamiltonian rather than in the Lagrangian form. In this representation all important information about the problem is contained in the local dispersion relation  $\Omega(x, y, k_x, k_y)$  of the linear operator. This function plays the role of the Hamilton's function in the indicated mechanical analogy.

In the WKB approximation the functional integral can be calculated by the steepest descent method, where the Green's function behavior is determined by the extremal trajectory governed by the Hamilton equations

$$\frac{dx}{d\tau} = -i \frac{\partial \Omega}{\partial k_x}, \quad \frac{dy}{d\tau} = -i \frac{\partial \Omega}{\partial k_y}, \quad (8)$$

$$\frac{dk_x}{d\tau} = i \frac{\partial \Omega}{\partial x}, \quad \frac{dk_y}{d\tau} = i \frac{\partial \Omega}{\partial y}.$$

This approximation is valid if the action  $S_{ext}$  at the extremal trajectory is large. Thus, the Green's function is just  $G \sim \exp(S_{ext})$  and the problem is reduced to the solution of the Hamilton equations for the given Hamilton's function  $\Omega(x, y, k_x, k_y)$ . Of course, this set of nonlinear Hamilton equations may still be difficult to solve.

### B. Local dispersion relation

The important point is that the local dispersion relation for this solidification problem is just the well-known local Mullins-Sekerka spectrum. Let us replace the interface of the needle crystal in the vicinity of its arbitrary point  $x, y, z = \zeta_0(x, y)$  by a piece of its tangential plane. For the short-wavelength perturbation of the form

$$\delta n \sim e^{\Omega t} e^{-ik_s s - ik_u u},$$

the local Mullins-Sekerka spectrum is

$$\Omega = \sqrt{k_s^2 + k_u^2} [\cos \Theta - \sigma(k_s^2 + k_u^2)] + ik_s \sin \Theta. \quad (9)$$

Here  $\Theta$  is the angle between the  $z$  axis and the local normal  $\hat{n}$ ;  $k_s$  and  $k_u$  are components of a wave vector along  $\hat{s}$  and  $\hat{u}$ ;  $\hat{s}$  and  $\hat{u}$  are the unit orthogonal vectors in the tangential plane; the unit vector  $\hat{s}$  lies in the tangential plane and in the normal plane  $(n, z)$ . The first two terms in Eq. (9) describe the Mullins-Sekerka unstable spectrum for the perturbation of an initially flat interface moving with the normal velocity  $\cos \Theta$ , with account being taken of the surface energy. The last term takes into account the tangential component of the velocity of liquid ( $\sin \Theta$ ) with respect to the unperturbed interface in the frame of reference moving with the dendritic tip with the velocity equal to 1.

### C. Transformation to Cartesian coordinates

The spectrum (9) is presented in the local orthogonal frame of reference  $n, s, u$ . It is convenient to rewrite it in the fixed Cartesian coordinates. The unit vectors  $\hat{n}, \hat{s}, \hat{u}$  have the following projections on the Cartesian coordinates  $(x, y, z)$ :

$$\begin{aligned} \hat{n} &= (\sin \Theta \cos \varphi, \sin \Theta \sin \varphi, \cos \Theta), \\ \hat{s} &= (\cos \Theta \cos \varphi, \cos \Theta \sin \varphi, -\sin \Theta), \\ \hat{u} &= (\sin \varphi, -\cos \varphi, 0), \end{aligned} \quad (10)$$

where  $\varphi$  is the angle between the  $x$  axis and the projection of the normal  $\hat{n}$  on the  $(x, y)$  plane.

The profile of the needle crystal is given by the equation

$$z = \zeta_0(x, y). \quad (11)$$

For this profile

$$\begin{aligned} \cos \Theta &= \frac{1}{\sqrt{1 + p^2 + q^2}}, \quad \sin \Theta = \frac{\sqrt{p^2 + q^2}}{\sqrt{1 + p^2 + q^2}}, \\ \cos \varphi &= \frac{-p}{\sqrt{p^2 + q^2}}, \quad \sin \varphi = \frac{-q}{\sqrt{p^2 + q^2}}, \end{aligned} \quad (12)$$

where  $p = \partial\zeta_0/\partial x$ ,  $q = \partial\zeta_0/\partial y$ . (We consider the part of the profile where  $\Theta$  and  $\varphi$  are positive.)

Let us introduce  $k_x$  and  $k_y$  instead of  $k_s$  and  $k_u$ , using the invariance of the scalar product:

$$k_s ds + k_u du = k_x dx + k_y dy, \quad (13)$$

where

$$ds = \hat{s} \cdot d\hat{\ell}, \quad du = \hat{u} \cdot d\hat{\ell}$$

and  $d\hat{\ell} = (dx, dy, dz \equiv pdx + qdy)$ . Thus we obtain  $k_s$  and  $k_u$  in terms of  $k_x$  and  $k_y$ :

$$\begin{aligned} k_s &= -\frac{pk_x + qk_y}{(p^2 + q^2)^{1/2} (1 + p^2 + q^2)^{1/2}}, \\ k_u &= \frac{-qk_x + pk_y}{(p^2 + q^2)^{1/2}}. \end{aligned} \quad (14)$$

The substitution of Eqs. (12) and (14) into Eq. (9) yields the dispersion relation  $\Omega(x, y, k_x, k_y)$ .

#### D. Approximations

Let us formulate the set of self-consistent approximations which we will use in the following analysis.

(i) We consider the behavior of  $G$  at the large distances from the tip,  $|Z| \gg 1$ . Eventually, this ensures the applicability of the above-mentioned WKB approximation.

(ii) On the other hand, according to Ref. [11], the effective noise is localized within a small region near the tip. This happens simply because the fluctuations that occur near the tip are the ones that have grown most by the time they are observed at the distance  $|Z|$ . Thus, we consider the source point to be located on the tip:  $X' = Y' = 0$ .

(iii) The main restriction of our calculation comes from the fact that any further analytical progress can be reached only for small values of  $y$ , i.e., close to the tip of the main arm in the cross section (Fig. 1). In this region the unperturbed interface of the needle crystal, which is given by Eqs. (4) and (5), can be written as

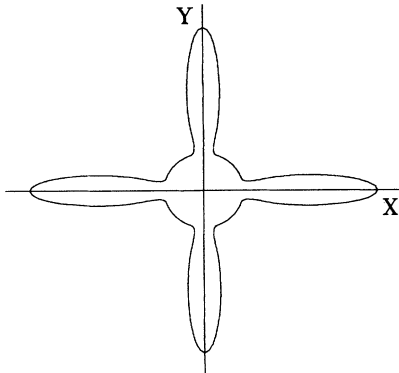


FIG. 1. The cross section of the dendrite.

$$\left(\frac{5}{3}|z|\right)^{3/5} - \frac{y^2}{\left(\frac{5}{3}|z|\right)^{1/5}} = x, \quad \frac{y}{|z|^{2/5}} \ll 1. \quad (15)$$

Here we have omitted the factor  $[\sigma_2^*(\alpha)/\sigma^*(\alpha)]^{1/5}$  in (4) and (5), which is very close to 1.

As shown below, the actual values of  $k_y(\tau) \sim y(\tau)$  are also small in the region of small  $y$ . For small  $y$  and  $k_y$ , we can expand the function  $\Omega$  to the second-order terms:

$$\Omega(x, y, k_x, k_y) = \Omega_0(x, k_x) + \Omega_1(x, y, k_x, k_y), \quad (16)$$

where

$$\Omega_1(x, y, k_x, k_y) = \frac{1}{2} Ay^2 + B y k_y + \frac{1}{2} C k_y^2. \quad (17)$$

Here  $\Omega_0$ ,  $A$ ,  $B$ , and  $C$  are the functions of  $x$  and  $k_x$  only. Straightforward but tedious calculations give for  $x \gg 1$  (or  $|z| \gg 1$ ) the following equations:

$$\Omega_0 = \frac{-ik_x}{p_0} \left[ 1 + i \frac{\sigma k_x^2}{p_0^2} + \frac{i}{p_0} \right], \quad (18a)$$

$$A = \frac{b^2 k_x}{p_0^2} \left[ 1 + \frac{3\sigma k_x^2}{p_0} + \frac{2i}{p_0} \right], \quad (18b)$$

$$B = -\frac{b}{p_0} \left[ 1 + \frac{3\sigma k_x^2}{p_0} + \frac{i}{p_0} \right], \quad (18c)$$

$$C = \frac{1}{k_x} \left[ 1 + \frac{3\sigma k_x^2}{p_0} \right], \quad (18d)$$

where

$$p_0 = (\partial\zeta_0/\partial x)_{y=0}, \quad b = (\partial^2\zeta_0/\partial y^2)_{y=0}.$$

These equations are derived for an arbitrary profile with extremum at  $y = 0$  and they are valid for  $|p_0| \gg 1$ . For our profile [Eq. (15)]

$$p_0 = -x^{2/3}, \quad b = -2x^{1/3}. \quad (19)$$

Using the approximation of small  $y$  and  $k_y$ , we can solve the Hamilton equations analytically by an iterative procedure.

### III. SOLUTION OF THE HAMILTON EQUATIONS

After substitution of Eqs. (16) and (17) into Eqs. (8), we obtain

$$\frac{dx}{d\tau} = -i \frac{\partial\Omega_0}{\partial k_x} - \frac{1}{2} i y^2 \frac{\partial A}{\partial k_x} - i y k_y \frac{\partial B}{\partial k_x} - \frac{1}{2} i k_y^2 \frac{\partial C}{\partial k_x}, \quad (20)$$

$$\frac{dy}{d\tau} = -i B y - i C k_y, \quad (21)$$

$$\frac{dk_y}{d\tau} = iAy + iBk_y. \quad (22)$$

Instead of the equation  $dk_x/d\tau = i\partial\Omega/\partial x$ , we use the relation (16) and the fact that for a Hamiltonian system  $\Omega$  does not depend on time  $\tau$  and depends on the initial and final points of the trajectory only. Thus, we can present this relation in the form:

$$\Omega_0(x, k_x) + \frac{1}{2}Ay^2 + Byk_y + \frac{1}{2}Ck_y^2 = \bar{\Omega}(X, Y, t). \quad (23)$$

We would like to find the optimal trajectory, that is, four unknown functions  $x(\tau)$ ,  $y(\tau)$ ,  $k_x(\tau)$ , and  $k_y(\tau)$ , which are governed by Eqs. (20)–(23) and by four boundary conditions:  $x(0) = X' = 0$ ,  $y(0) = Y' = 0$ ,  $x(t) = X$ , and  $y(t) = Y$ . In order to do this we use the following iterative strategy:

(i) The first step is to solve these equations for the case  $y(\tau) = 0$  and  $k_y(\tau) = 0$ . This gives the trajectory  $x(\tau)$ ,  $k_x(\tau)$  along the ridge of the side arm.

(ii) The second step is to find  $y(\tau)$ ,  $k_y(\tau)$  for the fixed functions  $x(\tau)$  and  $k_x(\tau)$  given by the first step.

(iii) Finally, we find the corrections to  $x(\tau)$ ,  $k_x(\tau)$  due to the functions  $y(\tau)$ ,  $k_y(\tau)$  given by the second step.

First of all, according to this strategy, we solve the problem for  $y(\tau) = 0$ ,  $k_y(\tau) = 0$ . From Eqs. (18a), (20), and (23), we find

$$k_x = ip_0\bar{\Omega} (1 - i/p_0 + i\sigma\bar{\Omega}^2) \quad (24)$$

and

$$\frac{dx}{d\tau} = -\frac{1}{p_0} \left( 1 + \frac{i}{p_0} - i3\sigma\bar{\Omega}^2 \right). \quad (25)$$

Here and below we use the smallness of the parameter  $1/p_0$  and the fact that  $\sigma\bar{\Omega}^2$  turns out to be of the order of  $1/p_0$ . For the subsequent calculations, we often need the main approximation only:

$$k_x \simeq ip_0\bar{\Omega}, \quad \frac{dx}{d\tau} \simeq -1/p_0. \quad (26)$$

The next step consists in the solution of the oscillator equations (21) and (22). We can derive one equation for  $y(\tau)$  from the two equations (21) and (22),

$$\ddot{y} - \frac{\dot{C}}{C} \dot{y} - y(AC - B^2 - i\dot{B} + iB\frac{\dot{C}}{C}) = 0, \quad (27)$$

where the dot denotes the derivative with respect to  $\tau$ . This equation can be solved in the WKB approximation. The asymptotic solution for large  $\tau$  satisfying the condition  $y(t) = Y$  is given by the relation

$$y(\tau) \simeq Y \frac{f(\tau)}{f(t)} \exp \left[ \int_t^\tau w(\tau') d\tau' \right], \quad (28)$$

where

$$w^2(\tau) = AC - B^2 - i\dot{B} + iB\frac{\dot{C}}{C} \quad (29)$$

and the prefactor  $f(\tau)$  obeys the equation

$$\dot{f} + \frac{1}{2} f \left( \frac{\dot{w}}{w} - \frac{\dot{C}}{C} \right) = 0. \quad (30)$$

In order to calculate  $w$  we use the relations (18b,c,d) and (26). In the approximation, where we drop terms  $i/p_0$  in (18b,c), the frequency  $w_0^2 \equiv AC - B^2 = 0$ . With these  $i/p_0$  terms we get

$$w_0 \equiv \sqrt{AC - B^2} = -b/p_0^2. \quad (31)$$

Calculating the additional terms in Eq. (29) in the main approximation, we find

$$w = w_0\beta, \quad (32)$$

$$\beta = \left[ 1 - i \left( \frac{db}{dx} \right) \frac{p_0^2}{b^2} (1 - 3\sigma\bar{\Omega}^2 p_0) \right]^{1/2}.$$

Now, from Eq. (21), we find the following relation between  $k_y(\tau)$  and  $y(\tau)$ :

$$k_y(\tau) = y(\tau) \frac{bk_x}{p_0} \left[ 1 - i \frac{(\beta - 1)}{p_0(1 - 3\sigma\bar{\Omega}^2 p_0)} \right]. \quad (33)$$

For the obtained asymptotic solution (33) we calculate  $\Omega_1$ :

$$\Omega_1 \equiv \frac{1}{2}Ay^2 + Byk_y + \frac{1}{2}Ck_y^2 = i \left( \frac{db}{dx} \right) \frac{y^2 k_x}{2p_0^2}. \quad (34)$$

Now we consider Eqs. (20) and (23) for  $k_x$  and  $dx/d\tau$  in the first approximation with respect to  $y^2$ :

$$\frac{dx}{d\tau} = -\frac{1}{p_0} \left[ 1 + \frac{i}{p_0} - i3\sigma\bar{\Omega}^2 - \frac{\beta b^2 y^2}{p_0^2} \right] \quad (35)$$

and

$$k_x = ip_0\bar{\Omega} \left[ 1 - \frac{i}{p_0} + i\sigma\bar{\Omega}^2 + \frac{1}{2} \left( \frac{db}{dx} \right) \frac{y^2}{p_0} \right]. \quad (36)$$

The integration of Eq. (35) gives

$$-t = \zeta_0(X, 0) [1 + i3\sigma\bar{\Omega}^2] - iX + \int_0^t (\beta b^2 y^2 / p_0) (dx/d\tau) d\tau. \quad (37)$$

Using Eq. (28), we calculate the last integral in Eq. (37) in the main approximation ( $\omega t \sim |p_0| \gg 1$ ). In this case the main contribution to the integral comes from its upper limit. Finally it gives

$$-t = \zeta_0(X, 0) [1 + i3\sigma\bar{\Omega}^2] - iX + \frac{1}{2} bY^2 (1 - \epsilon), \quad (38)$$

where  $\epsilon \sim 1/p_0$ .

#### IV. ACTION AT THE EXTREMAL TRAJECTORY

Now we can calculate the action  $S$  as defined by Eq. (7),

$$S(X, Y, t) = t\bar{\Omega} - i \int_0^X k_x dx - i \int_0^Y k_y dy. \quad (39)$$

Using relations (33), (36), and (38), we find

$$\begin{aligned} -i \int_0^X k_x dx &\equiv -i \int_0^t k_x \left( \frac{dx}{d\tau} \right) d\tau \\ &= \bar{\Omega} \left\{ \zeta_0(X, 0) (1 + i\sigma\bar{\Omega}^2) \right. \\ &\quad \left. - iX + \frac{1}{4} \left( \frac{db}{dx} \right) \frac{Y^2 p_0}{\beta b} \right\} \end{aligned} \quad (40)$$

and

$$\begin{aligned} -i \int_0^Y k_y dy &= -i \int_0^t k_y \left( \frac{dy}{d\tau} \right) d\tau \\ &= \frac{1}{2} b\bar{\Omega}Y^2 \left[ 1 - \frac{1}{p_0} + i\sigma\bar{\Omega}^2 \right. \\ &\quad \left. - i \frac{(\beta - 1)}{p_0(1 - 3\sigma\bar{\Omega}^2 p_0)} \right. \\ &\quad \left. - \frac{1}{2} \left( \frac{db}{dx} \right) \frac{p_0}{\beta b^2} \right]. \end{aligned} \quad (41)$$

Finally, one obtains for  $S$ :

$$\begin{aligned} S(X, Y, t) &= \bar{\Omega} \left\{ -i\zeta_0(X, 0) 2\sigma\bar{\Omega}^2 \right. \\ &\quad \left. + \frac{1}{2} bY^2 \left[ \epsilon - \frac{i}{p_0} + i\sigma\bar{\Omega}^2 \right. \right. \\ &\quad \left. \left. - i \frac{(\beta - 1)}{p_0(1 - 3\sigma\bar{\Omega}^2 p_0)} \right] \right\}. \end{aligned} \quad (42)$$

Equation (38) defines  $\bar{\Omega}$  as a function of  $X, Y$  and  $t$ :

$$\bar{\Omega}^2(X, Y, t) = -\frac{X}{3\sigma|\zeta_0(X, 0)|} \left\{ 1 + \frac{i\delta}{X} - i\frac{\epsilon}{2} \frac{bY^2}{X} \right\}, \quad (43)$$

where

$$\delta = t + \zeta_0(X, 0) + \frac{1}{2} bY^2. \quad (44)$$

Equations (42)–(44) are the main results and provide the expression for the action and, thus, for the Green’s function of the perturbation of an arbitrary steady-state crystal shape.

It is more convenient to present  $S$  as a function of  $Z, Y$  instead of  $X, Y$ . Using the shape equation (15), we get the action for our problem. A lengthy but straightforward calculation yields

$$S(Z, Y, t) = \frac{2(5/3)^{9/10}}{3\sqrt{3\sigma}} |Z|^{2/5} \left\{ 1 + \frac{3}{2} \frac{i\delta}{X_0(Z)} - \frac{3}{8} \frac{\delta^2}{X_0^2(Z)} - \frac{9}{4} \frac{Y^2}{X_0^{4/3}(Z)} \left( \sqrt{1 - i/9} - 1 \right) - \frac{3\alpha}{2} \frac{\delta Y^2}{X_0^{7/3}(Z)} \right\}, \quad (45)$$

where

$$X_0(Z) = \left( \frac{5}{3} |Z| \right)^{3/5}, \quad \delta = t + Z,$$

and

$$\begin{aligned} \alpha &\equiv -\text{Re} \left[ 3i \left( \sqrt{1 - i/9} - 1 \right) - \frac{5}{24} \frac{1}{\sqrt{1 - i/9}} \right] \\ &= 0.039381. \end{aligned}$$

Substituting  $X_0(Z)$  and  $\delta = t - |Z|$ , we find

$$\begin{aligned} S(Z, Y, t) &= \frac{2(5/3)^{(9/10)}}{3\sqrt{3\sigma}} |Z|^{2/5} \left\{ 1 + i\frac{3}{2} \left( \frac{3}{5} \right)^{3/5} \frac{(t - |Z|)}{|Z|^{3/5}} - \frac{3}{8} \left( \frac{3}{5} \right)^{6/5} \frac{(t - |Z|)^2}{|Z|^{6/5}} \right. \\ &\quad \left. - \frac{9}{4} \left( \frac{3}{5} \right)^{4/5} \left( \sqrt{1 - i/9} - 1 \right) \frac{Y^2}{|Z|^{4/5}} - \frac{3\alpha}{2} \left( \frac{3}{5} \right)^{7/5} \frac{Y^2(t - |Z|)}{|Z|^{7/5}} \right\}. \end{aligned} \quad (46)$$

In order to obtain this relation we have expanded Eqs. (42) and (43) in the small parameters

$$\frac{(t - |Z|)}{|Z|^{3/5}} \ll 1 \quad \text{and} \quad \frac{Y^2}{|Z|^{4/5}} \ll 1 \quad (47)$$

to the quadratic terms with respect to the first parameter and to the linear terms with respect to the other one. In the written terms, the  $\epsilon$  correction [see Eqs.(42)and(43)] does not appear at all. It appears only in the term proportional to  $Y^2(t - |Z|)^2$ , which describes the weak dependence of a correlation length on  $Y$ . We have not written the term  $iY^2(t - |Z|)$ , which corresponds to the weak dependence of the wavelength of oscillation on  $Y$ .

### V. SIDEBRANCHES AS A RESPONSE TO THERMAL FLUCTUATIONS

After the calculation of the action  $S$  at the optimal trajectory, we can write the Green's function as

$$G \sim \exp(S), \quad (48)$$

where a prefactor comes from the functional integration over the space close to the optimal trajectory. The noise-induced correction  $\xi_1(Z, Y, t)$  to the interface shape [the profile is described by the relation  $X = X_0(Z, Y) + \xi_1(Z, Y, t)$ ] is given by the general relation

$$\xi_1(Z, Y, t) = \int dZ' dY' \int_{-\infty}^t dt' G(Z, Y, t, Z', Y', t') \times \eta(Z', Y', t'), \quad (49)$$

where  $\eta$  is a stochastic field of noise at the interface. Formally,  $\eta$  is the inhomogeneous term in the linear equation

$$L \xi_1 = \eta,$$

where  $L$  is a linear operator which has the local spectrum (9) and the Green's function  $G$ .

The appropriate procedure for introducing thermal noise into a system of this kind is to add a fluctuating heat source to the thermal diffusion equation. The autocorrelation function for the source is chosen so as to reproduce the known thermodynamic fluctuations of the diffusion field. This procedure is described in detail by Langer in [11]. Let us just review here a few main points. The main contribution to the integral (49) over space variables  $Z', Y'$  comes from the tip region. This happens simply because the fluctuations that occur near the tip are ones that have grown most by the time they are observed at the point  $|Z|$ . Unfortunately, we cannot compute accurately the dependence of the Green's function on the source point, at least not by means of the WKB approximation that we have been using so far. Langer mentioned that all the missing information from the Green's function can be incorporated into a single numerical factor. Another point is that the fluctuations can be described by a white noise on the time scale of our problem.

Assuming the integration over space variables  $Z', Y'$  is performed, we can write

$$\xi_1(Z, Y, t) \sim \int_{-\infty}^t dt' G(Z, Y, t - t') \eta(t'). \quad (50)$$

Here  $G$  is given by Eqs. (46), (48) and

$$\langle \eta(t) \rangle = 0 \quad \text{and} \quad \langle \eta(t_1) \eta(t_2) \rangle = \bar{Q}^2 \delta(t_1 - t_2), \quad (51)$$

where the fluctuation strength  $\bar{Q}$  is given in ref. [11] as

$$\bar{Q}^2 = \frac{2k_B T^2 c_p D}{L^2 v \rho^4}. \quad (52)$$

From Eqs. (50) and (51), we find the correlation function

$$\langle \xi_1(Z_1, Y_1) \xi_1(Z_2, Y_2) \rangle \sim \bar{Q}^2 \int_0^\infty dt G(Z_1, Y_1, t) \times G(Z_2, Y_2, t). \quad (53)$$

For coinciding points ( $Z_1 = Z_2 = Z, Y_1 = Y_2 = Y$ ), we obtain the root-mean-squared amplitude for the sidebranches generated by thermal fluctuations,

$$\begin{aligned} \langle \xi_1^2(Z, Y) \rangle^{1/2} \sim \bar{Q} \exp \left\{ \frac{2(5/3)^{9/10}}{3\sqrt{3}\sigma} |Z|^{2/5} \right. \\ \times \left[ 1 - \frac{9}{4} \left( \frac{3}{5} \right)^{4/5} (\sqrt{1 - i/9} - 1) \right. \\ \left. \left. \times \frac{Y^2}{|Z|^{4/5}} \right] \right\}. \end{aligned} \quad (54)$$

Comparing Eq. (54) and Eq. (3.19) in Ref. [11], we conclude that the prefactor can be written as  $\bar{Q} \bar{C} \sigma^{1/8} g(Z, Y)$ , where  $\bar{C} (\sim 1)$  denotes the group of undetermined constant prefactors. The function  $g(Z, Y)$  describes a weak dependence of the prefactor on the coordinates and, for example, for the paraboloid shape, this function behaves as  $|Z|^{3/16}$  [11] and remains of order unity even far from the tip.

The estimation for the double-point correlation function at the points ( $Z_1, Y = 0$ ) and ( $Z_2, Y = 0$ ) gives for  $Z_1 \simeq Z_2 \simeq Z$

$$\begin{aligned} \langle \xi_1(Z_1, 0) \xi_1(Z_2, 0) \rangle &= \langle \xi_1^2(Z_1, 0) \rangle^{1/2} \langle \xi_1^2(Z_2, 0) \rangle^{1/2} \\ &\times \cos \left[ \frac{2\pi(Z_1 - Z_2)}{\lambda} \right] \\ &\times \exp \left[ - \frac{(Z_1 - Z_2)^2}{2\ell_c^2} \right], \end{aligned} \quad (55)$$

where

$$\begin{aligned} \ell_c^2 &= 4 \left( \frac{5}{3} \right)^{3/10} \sqrt{3\sigma} |Z|^{4/5}, \\ \lambda &= 2\pi \left( \frac{3}{5} \right)^{3/10} \sqrt{3\sigma} |Z|^{1/5}. \end{aligned} \quad (56)$$

## VI. DISCUSSION

Equation (54) describes an increase in the amplitude with the growth of the distance from the tip  $|Z|$ . This amplitude grows exponentially as a function of  $(|Z|^{2/5}/\sigma^{1/2})$ . At a fixed distance,  $|Z| = \text{const}$ , the amplitude slightly decays and oscillates with  $Y$ . The important result is that the amplitude of the sidebranches for the anisotropic needle grows faster than for the axisymmetric paraboloid shape. In the latter case it grows exponentially as a function of  $(|Z|^{1/4}/\sigma^{1/2})$  [11]. We think that this effect can resolve the puzzle that experimentally observed sidebranches have much larger amplitudes than can be explained by thermal noise in the framework of the axisymmetric approach [11]. Agreement with experiment would require at least one more order of magnitude in the exponential amplification factor. Indeed, we find that, for experimental values of  $\sigma = 0.02$  and  $|Z|$  where the first clear sidebranches can be seen [5], the ratio between the amplification factors for the actual anisotropic shape and the parabolic shape is

$$\exp(S_{anis})/\exp(S_{parab}) \simeq \begin{cases} 7 & \text{for } |Z| = 7 \\ 11 & \text{for } |Z| = 9. \end{cases}$$

The correlation length (or the width of the wave packet)  $\ell_c$  and the sidebranch spacing  $\lambda$  predicted by (56) depend on the distance from the tip  $|Z|$ . These dependencies are slightly different from those predicted by the axisymmetric approach [11], but the difference is not so crucial as the difference between the amplitudes, which grow exponentially with  $|Z|$ . For example, at the experimentally relevant distances  $|Z| = 7-9$  where the first clear sidebranches can be seen, the spacing predicted by (56)  $\lambda \simeq 2.0$ , which is in approximate agreement with experimental observations and with the spacing predicted by the axisymmetric approach [11] as well. As noted by Langer [11], the position at which the sidebranches appear (become visible) and their initial spacing depend (logarithmically) on the strength of the noise, and both are predicted to diverge slowly in the limit of small noise or small Peclet numbers  $P$ .

Far down from the tip the sidebranching deformations grow out of the linear regime and eventually start to behave like dendrites themselves. It is clear that the branches start to grow as free steady-state dendrites only at the distances from the tip which are of the order of the diffusion length, which, in turn, is much larger than the tip radius  $\rho$  in the limit of small  $P$ . It means that there exists the large range of  $Z$ ,  $1 \ll |Z| \ll 1/P$ , where the sidebranches grow already in the strongly nonlinear regime, but they do not behave as free dendrites yet. We can think of some fractal object where the length and thickness of the dendrites and the distance between them increase according to some power laws with the distance from the tip  $|Z|$ . The dendrites in this object interact due

to the competition in the common diffusion field. Some of them die and some continue to grow in the direction prescribed by the anisotropy. This competition leads to the coarsening of the structure in such a way that the distance between the surviving dendrites  $\lambda(Z)$  is adjusted to be of the same order of magnitude as the length of the dendrites  $l(Z)$ . In order to find the characteristic lengths of this structure we use the scaling arguments similar to those of Ref. [15]. First of all, we estimate the temperature field far away from the dendrite with sidebranches as the far field for the Ivantsov paraboloid [2],

$$u \sim \frac{\Delta}{\ln \Delta} \ln(\Delta r).$$

This formula is valid for  $|z| < r < 1/\Delta$ , where  $(r, z)$  are the cylindrical coordinates. The total heat flux per unit length of the main dendrite is equal to  $q \sim -2\pi D\Delta/\ln \Delta$ . On the other hand, this flux is equal to the total heat release due to the growth of the branches,  $q \sim 4\rho^2 \frac{d}{dt}(ls/\lambda)$ . Here  $t$  is time,  $t = |Z|\rho/v$ , and  $s(Z)$  is the characteristic area of the cross section of a branch, the factor 4 is due to the fourfold symmetry (we remind that all the lengths are measured in units of the tip radius of the main dendrite  $\rho$ ). As in Ref. [15], we assume the selection relation for the sidebranches to be the same as for a free dendrite [see Eq.(2)],  $2Dd_0/(v_b\rho_b^2) = \sigma^*$ , where the branch tip radius  $\rho_b \sim \rho s/l$ . Combining all these relations together and taking into account that  $\lambda \sim l$  and  $v_b = \rho dl/dt$ , we find that the distance between the sidebranching dendrites, their length and the branch cross section area grow as  $|Z|$ ,

$$\lambda(Z) \sim l(Z) \sim s(Z) \sim |Z|.$$

This result is self-consistent with our estimation of the temperature field at the large distances  $r > |z|$ . Thus, in this fractal object, the survived branches behave almost as free dendrites, but the coarsening takes place. The whole dendritic structure with sidebranches looks like a fractal object on the scale smaller than the diffusion length and as a compact object on the scale larger than the diffusion length [16]. The mean density of a solid phase in the compact structure is equal to undercooling  $\Delta$ .

## ACKNOWLEDGMENTS

One of us (E.B.) would like to thank Y. Couder and V. Hakim for useful and stimulating conversations regarding the fractality of the dendritic structure. We thank H. Müller-Krumbhaar for discussions. This work was supported in part by the Russian Basic Research Foundation (93-02-2113).

[1] For a review, see J.S. Langer, in *Chance and Matter*, Les Houches Lectures XLVI (Elsevier, New York, 1987); D. Kessler, J. Koplik, and H. Levine, *ibid.* **37**, 255 (1988); E.A. Brener and V.I. Melnikov, *Adv. Phys.* **40**, 53 (1991);

Y. Pomeau and M. Ben Amar, in *Solids Far From Equilibrium*, edited by C. Godrèche (Cambridge University Press, Cambridge, 1992).

[2] G.P. Ivantsov, *Dokl. Akad. Nauk SSSR* **58**, 567 (1947).

- [3] M. Ben Amar and E. Brener, *Phys. Rev. Lett.* **71**, 589 (1993).
- [4] E. Brener, *Phys. Rev. Lett.* **71**, 3653 (1993).
- [5] C. Huang and M.E. Glicksman, *Acta Metall.* **29**, 701 (1981); **29**, 717 (1981).
- [6] A. Dougherty, P.D. Kaplan, and J.P. Gollub, *Phys. Rev. Lett.* **58**, 1652 (1987).
- [7] J. Maurer, B. Perrin, and P. Tabeling, *Europhys. Lett.* **14**, 575 (1991).
- [8] A. Dougherty and R. Chen, in *Computational Crystal Growers Workshop*, edited by J. Taylor (AMS, Providence, RI, 1992) p. 31.
- [9] R. Pieters and J.S. Langer, *Phys. Rev. Lett.* **56**, 1948 (1986).
- [10] M. Barber, A. Barbieri, and J.S. Langer, *Phys. Rev. A* **36**, 3340 (1987).
- [11] J.S. Langer, *Phys. Rev. A* **36**, 3350 (1987).
- [12] E.A. Brener, S.V. Iordanskii, and V.I. Mel'nikov, *Zh. Eksp. Teor. Fiz.* **94**, 320 (1988) [*Sov. Phys. JETP* **68**, 2574 (1988)].
- [13] S.V. Iordanskii, *Zh. Eksp. Teor. Fiz.* **94**, 180 (1988) [*Sov. Phys. JETP* **68**, 1398 (1988)].
- [14] D. Kessler and H. Levine, *Acta Metall.* **36**, 2693 (1988).
- [15] R. Almgren, W-S. Dai, and V. Hakim, *Phys. Rev. Lett.* **71**, 3461 (1993).
- [16] E. Brener, H. Müller-Krumbhaar, and D. Temkin, *Europhys. Lett.* **17**, 535 (1992).